Journal of Electroanalytical Chemistry 950 (2023) 117855

Contents lists available at ScienceDirect

Journal of Electroanalytical Chemistry

journal homepage: www.elsevier.com/locate/jelechem

A conceptual, mathematical and quantitative reassessment of the Thin-film Flooded Agglomerate Model for air cathodes

Benedetto Bozzini [a,*], Ivonne Sgura [b]

[a] Department of Energy, Politecnico di Milano, via Lambruschini 4, 20156 Milano, Italy
[b] Department of Mathematics and Physics, via per Arnesano, Università del Salento, 73100 Lecce, Italy

A B S T R A C T

Design, fabrication, scale-up, operation and degradation analysis of GDEs electrode are complex operations, requiring a precise knowledge-base and quantitative guidelines. Mathematical tools are strongly needed for this purpose, but often they exhibit conceptual, formal and computational complexities that - in practice - are manageable only by modelling experts. Consequently, models are, in fact, not sufficiently exploited to support systematically metal-air battery research, development and control, as they would have the potentialities to do. Sometimes, experiments are essentially used just to validate models, rather than using models to direct experimental work. In order to enable the concrete integration of mathematical modelling with experimental work on GDEs for ORR, in this paper we present a conceptual restatement of a state-of-the-art model for ORR GDEs, in view of physico-chemical and mathematical perspicuity. In addition, we provide a simplified analytical solution, that enables straightforward and physically transparent parametric analysis, and a detailed description of the numerical solution of the full problem.

1. Introduction

Gas Diffusion Electrodes (GDE) for the Oxygen Reduction Reaction (ORR) are crucial components of metal-air batteries and chlor-alkali electrolysis with oxygen depolarized cathodes, owing their functional performance to the orchestration of electrocatalysis, mass-transport in liquid and gas phases, as well as ionic and electronic conductivity. Optimal synergy of these aspects - guiding GDE fabrication and operation, and enabling durability - relies on the porosity architecture.

In a field of science and technology with these characteristics, the cooperation of mathematical modelling and experimental activities - from material synthesis to electrochemical testing and operation in device ambient - is self-evident. Moreover, formalizing capabilities play a crucial role in allowing a fruitful use of the wide range of available imaging methods and spectroscopic approaches, liable to answer concrete and relevant questions, to build an appropriate knowledge base.

Indeed, rich and highly qualified literature exists on mathematical modelling of ORR GDEs, its experimental validation and its use for the rationalization of experimental results. Nevertheless, the intricacies of the physico-chemical theory underlying mathematical modelling, some mathematical complexities and the technicalities of numerical solutions are, in fact, hindering a systematic, parallel use of GDE models in experimental GDE studies.

The aim of this work is thus, on the one hand, to systematically re-examine a state-of-the-art model - expounded chiefly in [1,2], and, on the other hand, to clarify in a simple, but complete, self-contained and explicit way, the underlying physical-chemistry, the mathematical problem it leads to and the formal tools required to solve it. In view of this ambition, we are also proposing a simplified analytical solution, that captures the essence of the model, enabling a transparent grasp on quantitative aspects, in relation to the concrete values of the model constants and parameters. This paves the way to sensitivity analysis and parameter identification tasks - the importance of which for concrete model use in the analysis of experimental data cannot be over-emphasized -, that will be the object of a subsequent work. Not being the aim of this methodological work to develop a new model, we shall stick to the original Authors' choices and hypotheses, with all their advantages and drawbacks, commenting or improving which is out of the scope of the present contribution.

2. Mathematical modelling of the Gas Diffusion Electrode (GDE) for the Oxygen Reduction Reaction (ORR)

2.1. Literature background

The "Thin-Film Flooded Agglomerate Model" (TFAM) has been initially proposed in [1], employed in a range of contexts - detailed below -, and finally revisited in [2], in a validation framework based on *in operando* X-ray radiography. This model has been originally

* Corresponding author.
E-mail addresses: benedetto.bozzini@polimi.it (B. Bozzini), ivonne.sgura@unisalento.it (I. Sgura).

https://doi.org/10.1016/j.jelechem.2023.117855
Received 21 August 2023; Received in revised form 28 September 2023; Accepted 11 October 2023
Available online 13 October 2023

Nomenclature

Lower-case Latin letters

a	auxiliary constant [V], defined in Eq. (23)
$\widetilde{b}$	auxiliary constant [1], defined in Eq. (23)
c	concentration of electroactive reagent (solution-phase O_2 in this work) [mol m^{-3}]
c_{bulk}	bulk concentration of the electroactive reagent [mol m^{-3}]
c_o	concentration of electroactive reagent (solution-phase O_2 in this work) [mol m^{-3}], set to 1 mol m^{-3} in the numerical computations of this work
dS/dV	the surface available per unit volume in the porous active layer [m^{-1}]. NB if S is constant along z, dV/dS can be regarded as the increment along coordinate z., i.e. the length element along the coordinate $S{\cdot}dz = dV$.
i_{BV}	Butler-Volmer (electrokinetic) current density [A m^{-2}]
i_{ion}	ionic current density [A m^{-2}]
i_L	limiting current density [A m^{-2}]
i_o	exchange current density [A m^{-2}]
i_R	electrochemical reaction current density [A m^{-2}]
i_{tot}	total current density, applied externally in a galvanostatic experiment [A m^{-2}]
m	molality of NaOH in the electrolyte solution [mol(NaOH) kg(solution)$^{-1}$]
m_{bulk}	bulk molality of NaOH in the electrolyte [mol kg^{-1}]
n	number of electrons exchanged in the electrochemical reaction [eq mol^{-1}]
r_{ag}	agglomerate radius [m]
r_s	radius of the gas-filled pores of the GDL [m]
u_i	non-dimensional oxygen partial pressure in the i-th domain [1]
v_i	non-dimensional water partial pressure in the i-th domain [1]
x	general coordinate describing the 1D problem, without reference to a specific domain [m]
z	the coordinate describing the 1D active layer [m]
z'	the coordinate describing the 1D gas-diffusion layer [m]
z"	the coordinate describing the 1D boundary layer [m]
z_b	thickness of the 1D boundary layer [m]
z_s	thickness of the 1D gas-diffusion layer [m]
z_t	thickness of the 1D active layer [m]

Upper-case Latin letters

A	auxiliary constant [1], defined in Eq. (23)
A_1, A_2	auxiliary constants [1], defined in Eq. (S33)
B_a, B_c	anodic and cathodic Tafel slopes [V]
$D_{A,+}$	binary Maxwell-Stefan coefficient of water (A) and Na^+ (+) in the electrolyte phase [m^2/s]
$D_{A,-}$	binary Maxwell-Stefan coefficient of water (A) and OH^- (-) in the electrolyte phase [m^2/s]
$D_{i,k}^{eff}$	binary Maxwell-Stefan coefficient of species i and k in the porous GDL and RL [m^2/s]
D_i^{eff}	Knudsen diffusion coefficient of species i [m^2/s], defined in Eq. (1).
$D_i^{eff,l}$	effective diffusion coefficient of the electroactive species i in the electrolyte [m^2/s]
D_i^l	diffusion coefficient of the electroactive species i in the electrolyte [m^2/s]
$D_{i,k}^g$	binary Maxwell-Stefan coefficient of species i and k in the gas phase of the BL [m^2/s]
F	Faraday constant [C eq^{-1}]
H	reciprocal of Henry's constant [N m/mol]
M_A	molar weight of H_2O [kg mol^{-1}]
M_i	molar weight of species i [kg mol^{-1}]
N_i	flux of the i-th gas, without reference to a specific domain [kg mol^{-1}]
N_i^j	flux of i-th gas in the j-th phase [mol m^{-2} s^{-1}]
P_i	partial pressure of i-th gas [N m^{-2}]
$P_{i,ext}$	partial pressure of i-th gas in the ambient external to the GDE [N m^{-2}]
P_T	total pressure of the gas mixture [N m^{-2}]
R	gas constant [N m K^{-1} mol^{-1}]
T	absolute temperature [K]

Lower-case Greek letters

α_{BL}	auxiliary constant [1], defined in Eq. (30)
α_{GDL}	auxiliary constant [1], defined in Eq. (42)
α_{RL}	auxiliary constant [m s/mol], defined in Eq. (59)
β	auxiliary constant, defined in Eq. (S6)
B_1	auxiliary constant, defined in Eq. (S14)
B_2	auxiliary constant, defined in Eq. (S19)
β_{BL}	auxiliary constant [1], defined in Eq. (31)
β_{GDL}	auxiliary constant [1], defined in Eq. (43)
β_{RL}	auxiliary constant [m s/mol], defined in Eq. (60)
γ	activity coefficient of NaOH [1]
γ_{BL}	auxiliary constant [1], defined in Eq. (32)
γ_{GDL}	auxiliary constant [1], defined in Eq. (44)
γ_{RL}	auxiliary constant [m s/mol], defined in Eq. (61)
δ	concentration boundary layer thickness or, in the case of a porous electrode, the equivalent for mass-transport at a triple-phase boundary (see specific discussions in the text body) [m]
ε_{GDL}	auxiliary constant [1], defined in Eq. (45)
ε_{RL}	auxiliary constant [m s/mol], defined in Eq. (46)
ε_n	active layer porosity [1]
ε_s	gas diffusion layer porosity [1]
ε_t	porosity of the gas region of the reaction layer porosity [1]
ζ	the non-dimensional coordinate describing the 1D active layer [1]
ζ'	the non-dimensional coordinate describing the 1D gas-diffusion layer [1]
ζ"	the non-dimensional coordinate describing the 1D boundary layer [1]
η	overvoltage [V]
κ_{ion}	ionic conductivity for the free electrolyte [S m^{-1}] = [A V^{-1} m^{-1}]
κ_{ion}^{eff}	effective ionic conductivity for the electrolyte in a porous structure [S m^{-1}] = [A V^{-1} m^{-1}]
λ	relaxation length of the electroactive species concentration within the active layer [m^{-1}]
M	auxiliary constant [1], defined in Eq. (S35)
μ_N	chemical potential of NaOH [J/mol]
ρ	density of the electrolyte solution [kg(NaOH solution) m^{-3}]
σ	electronic conductivity [S m^{-1}] = [A V^{-1} m^{-1}]
$\widetilde{\tau}$	auxiliary constant [m], defined in Eq. (23)
τ_n	active layer tortuosity factor [1]
τ_s	gas diffusion layer tortuosity factor [1]
τ_t	tortuosity factor of the gas region of the reaction layer porosity [1]

Upper-case Greek letters

Φ_{el}	potential of the electronically conducting phase [V]
Φ_{ion}	potential of the ionically conducting phase [V]

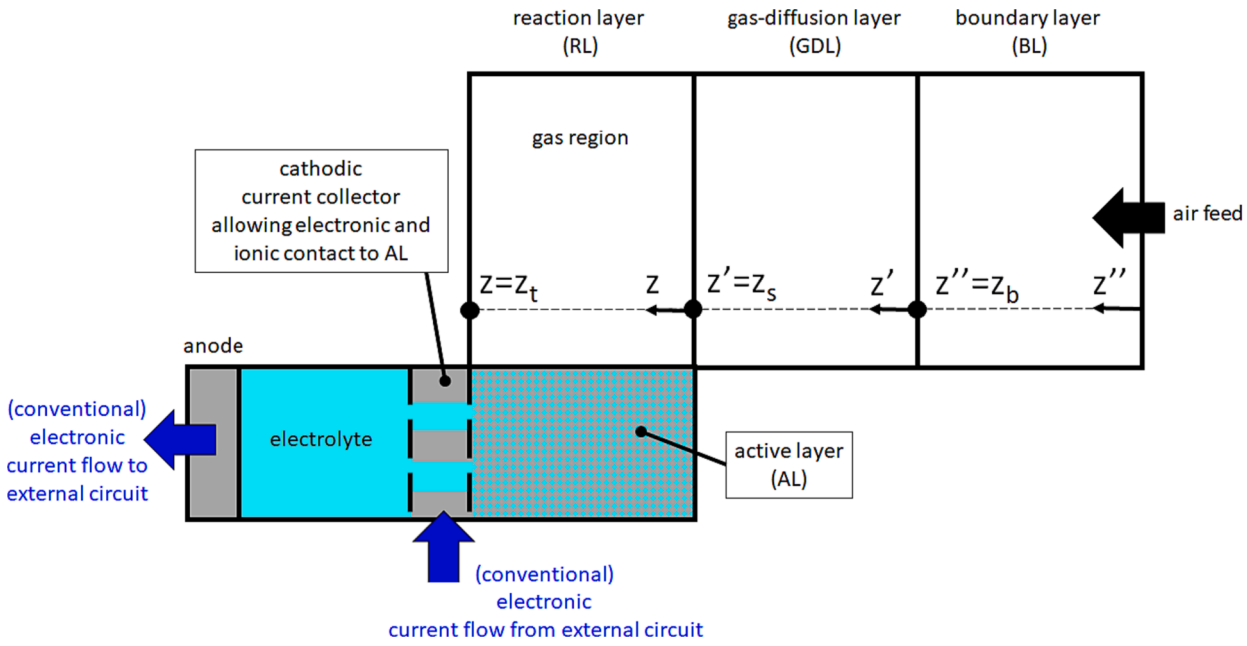

Fig. 1. Schematic of 1D gas-diffusion electrode and of the integration domains for the model. The regions colour-coded in white and light-blue contain gas and electrolyte, respectively both in the case of the active layer.

developed as a general tool to describe the operation of ORR GDEs for alkaline fuel cells, metal-air batteries and chloralkali electrolysis [3–5]. General literature agreement considers TFAM as the state-of-the-art model in the field [6,7].

Early GDE modelling, dating back to the 60′s, followed four main approaches: (i) accounting for porosity on two key length-scales [8], (ii) combining descriptors of porosity with the thin electrolyte film model [9–11]; (iii) considering a flooded porous domain [12,13] and (iv) outlining a flooded agglomerate [14]. The last approach was extended incorporating thin film mass transport into the flooded agglomerate model [15–20], yielding the thin-film agglomerate model (TFAM) that is the object of this work. The TFAM version of [1,2] is an original elaboration and extension of the above-mentioned previous work, targeting - in an effective-medium framework -, the steady-state galvanostatic operation of an isothermal ORR GDE. Architectural GDE parameters (thickness, porosity, tortuosity, ionic conductivity, electronic conductivity) are accounted for, together with electrokinetics (through Butler-Volmer parameters), multi-component mass-transport in the gas (O_2, H_2O and N_2) and liquid (O_2, H_2O, Na^+ and OH^-) phases, in the latter case also considering concentrated-electrolyte effects [21].

The TFAM was later extended to non-isothermal [22] and dynamic [7,23] cases. Moreover, this effective-medium approach was employed as the starting point of microscopic modelling of electrolyte imbibition into solid microstructures [24].

Regarding the combination of experimental with TFAM, the model was employed for the following studies: (i) assignment of numerical parameter values for the GDE of a Li-O_2 battery [25]; (ii) interpretation of experimental O_2-depolarized cathode data [23,26–28]; (iii) discussion of experimental CO_2 reduction GDE results [29], based on an application of the model to the corresponding reactions and mass-transport processes; (iv) rationalization of experimental data on electrolyte distribution into GDEs [30]. Finally, the activities of H_2O and OH^-, required by the model, were measured with SECM in [31].

For completeness, it is also worth recalling, that other important ORR GDE models are present in the literature of continuum [32,33], mesoscopic [34] and microscopic [35] types, an analysis of which is beyond the scope of the present study.

2.2. Physico-Chemical and geometrical structure of the model

The standard TFAM consists of a 1D-1D description of an ORR GDE in contact with the liquid electrolyte, the gas phase and the current collector, whereby a 1D model accounts for space-dependence along the electrode thickness (between the current collector and the free electrolyte or separator phase), that is combined with a second 1D model for the agglomerate extending perpendicularly to the electrode thickness. The GDE is schematized as the sequence of a stagnant gas-diffusion boundary-layer (BL), a porous gas-diffusion layer (GDL) and a reaction-layer (RL) consisting of a gas region and an active-layer (AL). The AL is a continuum description of the condensed phases present in the RL, i.e. of the “flooded aggregate” mentioned in the model acronym. Otherwise: the composite consisting of the solid electronically percolating network of electrocatalyst and corresponding electronically conducting support, intertwined with the liquid ionically percolating network of electrolyte, saturated with O_2. The model zones and the integration domain of the model equations are depicted in Fig. 1, where - for ease of reference - we keep the same axis conventions and symbols of [1]. All symbols are listed and explained in the Nomenclature table. Of course, being an electrode model, TFAM does not account for the electrolyte and the anode of the device in which it is meant to operate, while it describes gas transport from the air reservoir to the AL where O_2 is reduced. In a follow-up work, we shall integrate the GDE information in a model for the electrochemical response of the whole metal-air battery.

2.2.1. Model assumptions

In this work, coherently with [1,2], we shall consider a 1D, stationary and isothermal model for galvanostatic GDE operation. The structure of the TFAM equations and their solutions, detailed below, rely on the following assumptions.

(i) The total pressure P_T in all gas regions of the GDE (BL, GDL and gas region of RL in Fig. 1) is equal, and it consists of the sum of the partial pressures of oxygen, nitrogen and water vapour, whatever their local values: $P_{O_2} + P_{N_2} + P_{H_2O} = P_T = const.$ It should be noted here that this assumption is liable to be formally incompatible with specific choices of the mass-transport model (see below the Gas Transport Section).

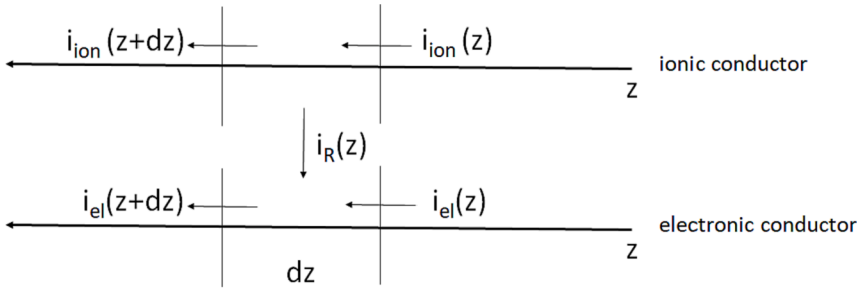

Fig. 2. Schematic of current density balance for the 1D GDE model.

(ii) Since nitrogen does not react, its flux is everywhere equal to zero: $N^g_{N_2} \equiv 0$.
(iii) Water exchange between the electrolyte and the gas phases is at equilibrium, whence water flux in the gas phase is everywhere equal to zero: $N^g_{H_2O} \equiv 0$.
(iv) Phase exchange for O_2 between the gas region and the liquid phase of the AL is at equilibrium. It is worth noting here that this equilibrium assumption accounts for the supply of O_2 from the air reservoir to the reaction site. In fact, since O_2 present in the liquid phase of the AL is consumed by the electrochemical reaction running at the electrocatalyst-electrolyte interface within the AL, a finite O_2 flux develops across the whole GDE. Of course, the phase-exchange equilibrium hypothesis, adopted in the reference works [1,2], is a rather crude one: nevertheless, it enables a simple description of O_2 transport within the AL, able to capture the essential quantitative aspects of electrochemical GDE performance.
(v) The electrolyte is homogeneous (i.e. the NaOH concentration is constant) outside the GDE.
(vi) The four-electron ORR mechanism applies, implying optimal electrocatalysts, e.g. by Ag or α-MnO_2, and the electrochemical reaction rate is first-order in dissolved O_2 concentration.

2.2.2. *Modelling of GDE architecture*

The BL is an unstructured stagnant layer, of thickness z_b, lying between the air supply chamber and the GDL.

The GDL, of thickness z_s, consists of gas-filled pores of radius r_s with porosity ε_s and tortuosity factor τ_s. r_s is employed in the evaluation of the Knudsen diffusion coefficient of species i, D_i^{eff} (see below for details on the use of this model constant in the mass-transport equation), according to the kinetic theory of gases, with:

$$D_i = \frac{2}{3}\cdot r_s \cdot \sqrt{\frac{8RT}{\pi M_i}} \tag{1}$$

ε_s and τ_s are used in the definition of the effective diffusion coefficient $D_{i,k}^{eff}$ and of the binary Maxwell-Stefan coefficients for species i and k, $D_{i,k}^{eff}$ in the GDL domain:

$$D_i^{eff} = \frac{\varepsilon_s}{\tau_s}\cdot D_i \tag{2.1}$$

$$D_{i,k}^{eff} = \frac{\varepsilon_s}{\tau_s}\cdot D_{i,k} \tag{2.2}$$

$D_{i,k}$ being the binary free diffusion coefficient for the gas phase, that can be estimated, e.g. with the program "Binary Diffusion Coefficients for Gases" of the Wolfram Demonstration Projects accessible at the website [36], that also details the equations implemented and their physico-chemical background.

The gas region of the RL, similarly to the GDL, is schematized as a porous layer of thickness z_t, consisting of gas-filled pores of radius r_t with porosity ε_t and tortuosity factor τ_t. There three geometric porosity parameters are used to estimate effective diffusion coefficients for the gas region of the RL, replacing the appropriate numerical values in Eqs. (2.1) and (2.2).

The AL region of the RL is described as a porous layer, again of thickness z_t. The AL pores are filled with electrolyte. The porous structure is modelled as a porous solid matrix - consisting, in general of electrocatalyst and electronically conducting additive (e.g. Ag nanoparticles, as in GDE for chlor-alkali electrolysis [1] or α-MnO_2 and carbon black, as in some GDEs for zinc-air batteries [37]) - with porosity ε_n and tortuosity factor τ_n. The geometry of the solid matrix (or "agglomerate") is described as an array of cylinders, lying along the z axis, of length z_t and radius r_{ag}.

Following [1], the specific electrochemically active surface area, referred to the total volume of the active layer is:

$$\frac{dS}{dV} = \frac{2}{r_{ag}}\cdot(1-\varepsilon_t). \tag{3}$$

The rationale of this expression is that the surface-to-volume ratio of cylinders of radius r_{ag}, (i.e. $2/r_{ag}$) is weighted with the volume fraction of the RL occupied by the AL (i.e.: $1\text{-}\varepsilon_t$).

Following [1], the AL porosity ε_n is modelled as:

$$\varepsilon_n = \frac{\varepsilon_s - \varepsilon_t}{1-\varepsilon_t} \tag{4}$$

the physical meaning of which is the RL porosity, filled with electrolyte. The rationale of this definition is that the RL is fabricated by filling a scaffold structure with the same geometry of the GDL of porosity ε_s, with a porous solid composite of gas-filled porosity ε_t. The liquid-filled fraction ε_n of the RL is thus defined as the fraction of the geometrical volume occupied by the whole RL, that is not filled with gas (i.e. that is filled with the solid and liquid constituents of the AL: $\varepsilon_s\text{-}\varepsilon_t$), divided by the volume-fraction of the RL alone that is not filled with gas ($1\text{-}\varepsilon_t$). The porosity and tortuosity of the AL are employed to estimate the effective diffusion coefficient of O_2 in the liquid electrolyte phase:

$$D_{O_2}^{eff,l} = \frac{\varepsilon_n}{\tau_n}\cdot D_{O_2}^{l} \tag{5}$$

as well as the effective ionic conductivity κ_{ion}^{eff} (see below Eq. (14)).

2.3. *Model equations*

The TFAM equations involve the coupled solution of the overvoltage distribution problem - accounting for the electrode voltage response to the imposed galvanostatic polarization - in the RL and of the mass-transport problems in the BL, GDL and RL. The applied current controls the mass-transport problems through flux terms. The mass-transport problems in the BL and GDL are decoupled from the overvoltage distribution problem and provide the boundary conditions for the coupled overvoltage distribution and mass-transport problems in the RL. In this Section, we shall first expound the overvoltage distribution problem in the RL and subsequently the mass-transport problems in the three model domains.

2.3.1. Overvoltage distribution

The overvoltage distribution in the electrochemically active region of a GDE, the AL in the present case, is an application of the divergence theorem, referring to the flow of electrons in the electronically and ionically conducting branches. The rationalization and implementation of this problem for a porous electrode in the continuum approximation is a classic in electrochemical mathematical modelling and electrochemical engineering, the conceptual framework of which has been set and consolidated in a series of seminal papers, among which, without any claim of completeness, we can mention [38–49]. Notwithstanding this time-honoured scientific history, the field is still actively investigated in diverse fields of electrochemistry (e.g. [50–52]).

Within the steady-state 1D description adopted in this work, the divergence theorem, or current–density (I [A m^{-2}]) balance, can be recast in the form corresponding to the scheme of Fig. 2 – referring to the GDE element of length dz – and expressed in Eqs. (6) and (7), where i_{el} and i_{ion} refer to the electronic and ionic current densities, respectively, i_R is the electrochemical reaction current density and j_R is the electrochemical volumetric current density [A m^{-3}], i.e. the electrical expression of the local reaction rate [mol m^{-3}]. Here, we adopt the common sign convention for the current, referring to a flux of positive charge carriers: in this case, the conventional cathodic ORR current density i_R flows from the ionic conductor to the electronic one.

$$i_{el}(z+dz) - i_{el}(z) = j_R(z)\mathrm{d}z \tag{6}$$

$$i_{ion}(z+dz) - i_{ion}(z) = -j_R(z)\mathrm{d}z. \tag{7}$$

At this point of our treatment, in which we refer to current density balances in general, the sign of the current is meant as an algebraic quantity and is left unspecified. The definition of the sign of i_R will be provided below, where ORR will be considered specifically (see Eqs. (16)–(18)). To more clearly handle electrochemical concepts, it is convenient to represent the electrochemical reaction current in terms of a surface-specific current density i_R [A m^{-2}] rather than the volume-specific one j_R [A m^{-3}] adopted in Eqs. (6) and (7). This conversion can be straightforwardly carried out in terms of the volume-specific active surface, defined in Eq. (3), whence:

$$j_R = i_R \cdot \frac{dS}{dV} \tag{8}$$

Thus, expanding the electronic and ionic current densities to first order, Eqs. (6) and (7) can be restated as Eqs. (9) and (10).

$$\frac{di_{el}}{dz} - i_R(z)\cdot\frac{dS}{dV} = 0 \tag{9}$$

$$\frac{di_{ion}}{dz} + i_R(z)\cdot\frac{dS}{dV} = 0. \tag{10}$$

Current density conservation implies that:

$$i_{el}(z) + i_{ion}(z) = i_{tot} \tag{11}$$

where i_{tot} is the total, externally applied (constant) current density in the galvanostatic experiment. Electron and ion fluxes (i.e. electronic and ionic current densities) in the electronic conductor, can be described in terms of migration, because the electrochemically reacting species O_2 is neutral and the change in ionic concentration resulting from ORR in an alkaline electrolyte is negligible in terms of ion transport, whence the diffusive term is not required in the expression for the ionic flux.

$$-\sigma\cdot\frac{d\Phi_{el}}{dz} = i_{el}(z) \tag{12}$$

$$-\kappa_{ion}^{eff}\cdot\frac{d\Phi_{ion}}{dz} = i_{ion}(z) \tag{13}$$

where σ is the electronic conductivity of the solid fraction of the AL and κ_{ion}^{eff} the effective ionic conductivity of the electrolyte-filled porous network of the AL, that can be estimated as follows from the ionic conductivity of the free electrolyte, the porosity of the AL ε_n and the flooded volume fraction 1-ε_t, with the same consideration that led to Eqs. (3) and (4):

$$\kappa_{ion}^{eff} = \kappa_{ion}\cdot\frac{\varepsilon_n}{\tau_n}\cdot(1-\varepsilon_t). \tag{14}$$

$\varepsilon_n\cdot(1-\varepsilon_t)$ quantifies the electrolyte-filled volume fraction of the AL and τ_n accounts for the effective length of ionic paths, due to tortuosity. It is worth noting that, in this model, the electronic conductivity σ is regarded as invariant with respect to changes in porosity because the properties of the electronically conducting framework are not affected by the processes typically altering porosity in the processes of interest (e.g. pore clogging with carbonate precipitates), that, instead, crucially affect the ionic conductivity, that, consequently ought to be modelled as an effective quantity.

Note that Eqs. (12) and (13) are written, again, according to the customary electrical sign convention (a negative potential flux drives a flux of positive charge-carriers). Then: (i) considering κ_{ion}^{eff} and σ constant, (ii) defining the overvoltage:

$$\eta = \Phi_{el} - \Phi_{ion} - E_{eq} \tag{15}$$

with E_{eq} the equilibrium potential of the ORR - under the hypothesis that $\frac{d^2E_{eq}}{dz^2} = 0$, i.e. that the dependency of E_{eq} on p_{O_2} and [OH^-] can be linearized -, and (iii) inserting Eqs. (12) and (13) into Eqs. (9) and (10), one obtains:

$$\frac{d^2\eta}{dz^2} = i_R\cdot\frac{\sigma+\kappa_{ion}^{eff}}{\sigma\cdot\kappa_{ion}^{eff}}\cdot\frac{dS}{dV} \tag{16}$$

The sign convention for η is again in keeping with the sign conventions for the current adopted above: cathodic $\eta < 0$ drives the conventional (i.e. formally considered to be carried by positive charges) i_R from the ionic to the electronic conductor, corresponding to cathodic electron flow (i.e. a negative conventional current) from the electronic to the ionic conductor. It is worth noting that the absence of a diffusive term in the ionic current for the case at stake of a GDE, allows to combine Eqs. (12) and (13) directly into Eq. (16), in which the unknown is the overvoltage η, the electrically relevant quantity for the electrochemical problem at hand. In this case it is therefore not necessary, as instead in a general electrochemical problem, to solve Φ_{el} and Φ_{ion} individually, to derive η, that, in turn, must be fed to the electrochemical reaction rate term i_R.

A convenient way of expressing i_R as a function of overvoltage η and reagent (O_2 in this case) concentration c, accounting for charge-transfer and mass-transport from the pore bulk to the electrochemically active pore surface, is the Gileadi approximation (see, e.g, [53] for a comprehensive presentation and discussion):

$$i_R(\eta,c) = \frac{i_{BV}(\eta,c)\cdot i_L(c)}{i_{BV}(\eta,c) + i_L(c)} \tag{17}$$

with i_{BV} the Butler-Volmer current density in Eq. (18), expressing charge-transfer controlled kinetics, and i_L the limiting current density. It should be noted that, for the case of a cathodic reaction, $i_R \le 0$, $i_{BV} \le 0$ and $i_L \le 0$.

$$i_{BV}(\eta,c) = \frac{c}{c_o}\cdot i_o\cdot\left(e^{\eta/B_a} - e^{-\eta/B_c}\right) \tag{18}$$

with c_o a reference concentration, i_o the exchange current density and B_a, B_c the anodic and cathodic Tafel slopes, respectively. It is worth noting that, in the case of a cathodic process, $\eta \le 0$, whence, with $i_o > 0$, it results that $i_{BV} \le 0$.

The limiting current density can be approximated as:

$$i_L(c) = nF\cdot\frac{D_{O_2}^l}{\delta}\cdot c \tag{19}$$

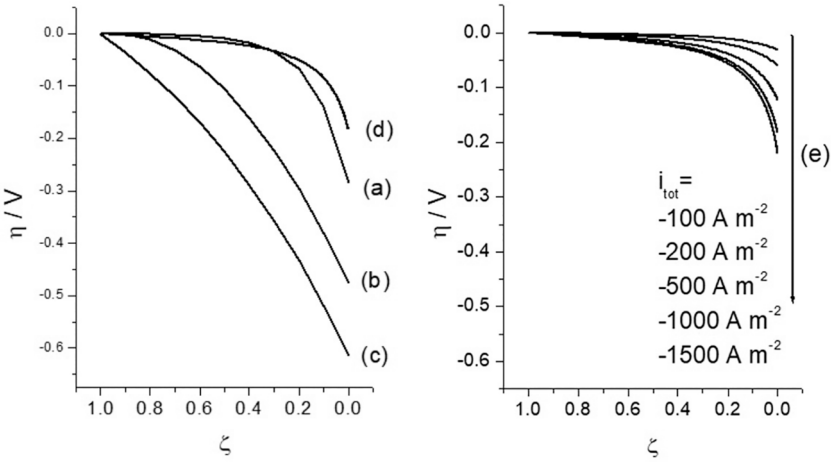

Fig. 3. Selection of the approximate solution of the overvoltage distribution (Eqs. (16) and (20)), plotted as a function of the normalized axis $\zeta = z/z_t$ of the RL region (see Fig. 1). (a-c) Analytical solutions presented in Section S1 of the Supplementary Material. (a) Constant reagent concentration, charge-transfer control and linearized charge-transfer kinetics (Section S1.1). (b) Mass-transport control with constant reagent concentration: analytical solution (Section S1.2). (c) Mass-transport control with exponential variation of reagent concentration: analytical solution (Section S1.3). (d) Mixed control with exponential variation of reagent concentration: numerical solution (Section S2). (e) Same as Plot (d), but with different values of the applied current density i_{tot}. The numerical values of the model parameters used for the computations are presented and commented in Table S1 of the Supplementary Material. For Plot (e), apart from the indicated values of the applied current density i_{tot}, the parameters values are the same as for Plot (d).

where n the number of electrons exchanged in the electrochemical reaction ($n = 4$, according to hypothesis (vi)), F the Faraday constant, $D^l_{O_2}$ the diffusion coefficient of the electroactive species in the free electrolyte and δ the effective concentration boundary layer thickness for mass-transport at the triple-phase boundary. Of course, in the case of a cathodic reaction, $i_L \leq 0$ and this can be expressed by the numerical setting $n = -4$.

Combining Eqs. (17)–(19), one obtains:

$$i_R(\eta, c) = c \cdot \frac{\frac{i_o}{c_o} \cdot \left(e^{\eta/B_a} - e^{-\eta/B_c}\right) \cdot nF \cdot \frac{D^l_{O_2}}{\delta}}{\frac{i_o}{c_o} \cdot \left(e^{\eta/B_a} - e^{-\eta/B_c}\right) + nF \cdot \frac{D^l_{O_2}}{\delta}} \tag{20}$$

The overvoltage distribution problem, thus consists in merging Eqs. (16) and (20). The resulting second-order ODE can be solved with the boundary conditions Eqs. (21) and (22):

$$|\eta|(z_t) = 0 \tag{21}$$

expresses the fact that, by construction, $i_R = 0$ since the electrochemical reaction cannot run at the current-collector / active-layer interface (see Fig. 1, position $z = z_t$), where the catalyst is absent, the current – that has to be continuous with that flowing in the current collector – is entirely electronic in nature and electrochemical equilibrium conditions prevail. An alternative, physically equivalent approach, solution of the boundary-value problem, would be that of setting the first derivative of η as directly proportional to the electronic current, as proposed in the framework of SOFC modelling with a slightly different domain geometry in [54].

$$\left.\frac{d|\eta|}{dz}\right|_{z=0} = -\frac{i_{tot}}{\kappa^{eff}_{ion}} \tag{22}$$

expresses the fact that at the active-layer / electrolyte interface (see Fig. 1, position $z = 0$) all the current applied to the electrode – that has to be continuous with that flowing in the electrolyte collector – has fully converted into ionic current.

The full problem can be solved only if the dissolved O_2 concentration distribution $c(z)$ is known. In general, this must be solved with the coupled mass-transport equation, discussed below. Nevertheless, instructive independent solutions of the overvoltage distribution problem can be obtained, with appropriate hypotheses on the $c(z)$. In the Supplementary Material, we report a series of approximate analytical (Section S1) and numerical (Section S2) solutions, that are compared in Fig. 3. Specifically, the Panels of Fig. 3 report examples of the analytical and numerical solutions of the overvoltage distribution problem, presented in Sections S1.1, S.1.2 and S1 and S2 of the Supplementary Material. All approximate solutions yield qualitatively similar overvoltage profiles. The quantitative details of the η (z) dependence and the sensitivity to the model parameters can be straightforwardly derived for the analytical solutions. In particular, it is worth noting that the analytical solutions of the approximations implying mass-transport control do not yield physical solutions of the overvoltage if the parameters describing active layer architecture δ, z_t and r_{ag} are set to the values corresponding to pristine conditions, while η values in the experimentally expected range are recovered if value corresponding to damaged active layer are employed. As expected, this outcome suggests that pure mass-transport control is typically not attained in an AL with a correct architecture.

As far as the numerical solution of Eq. (S20) is concerned, inspection of parameter sets in the physically meaningful range reveals that the η (ζ) ($\zeta = z/z_t$ being the non-dimensional RL coordinate) profiles can be accurately approximated with the analytical form:

$$\eta(1-\zeta) \cong a + \tilde{b} \cdot (1-\zeta) + A \cdot exp\left(\frac{1-\zeta}{\tilde{\tau}}\right) \tag{23}$$

that can be employed for the development of semi-analytical approximate solutions, that will be discussed below. The dependence of the formal parameters ($a, \tilde{b}, A, \tilde{\tau}$) on the physical model parameters is detailed in Section S3 of the Supplementary Material.

2.3.2. Gas transport

The gas of interest in this context is air, for the case of metal-air batteries, whereby mass transport in the gas phase for the three domains of interest (BL, GDL and gas region of the RL of Fig. 1) involves O_2 - the species that reacts in the AL of the RL -, together with N_2 and H_2O. It is worth noting that pure O_2 is instead employed for chlor-alkali electrolysis. Since the total pressure P_T is assumed to be constant (Assumption (i)), only two independent mass-transport problems have to be formulated. After [1], the mass-transport models adopted in this work are detailed below. A boundary layer (BL) develops between the well-mixed region of the gas chamber and the gas diffusion layer (GDL) region of the GDE. Gas transport in the BL can be modelled with

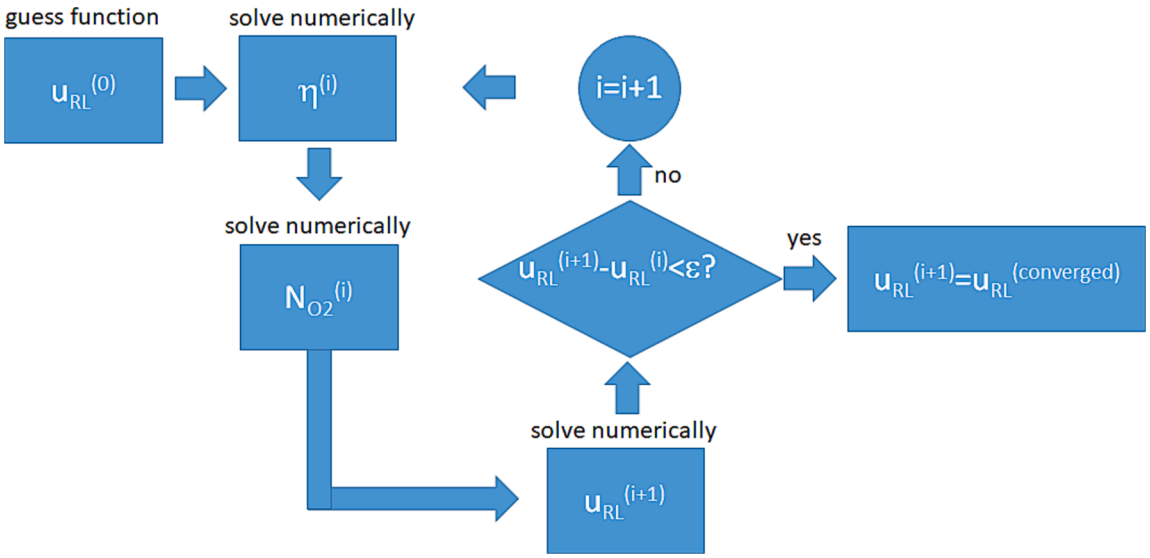

Fig. 4. Conceptual workflow of the self-consistent iterative scheme for the numerical solution of the TFAM model.

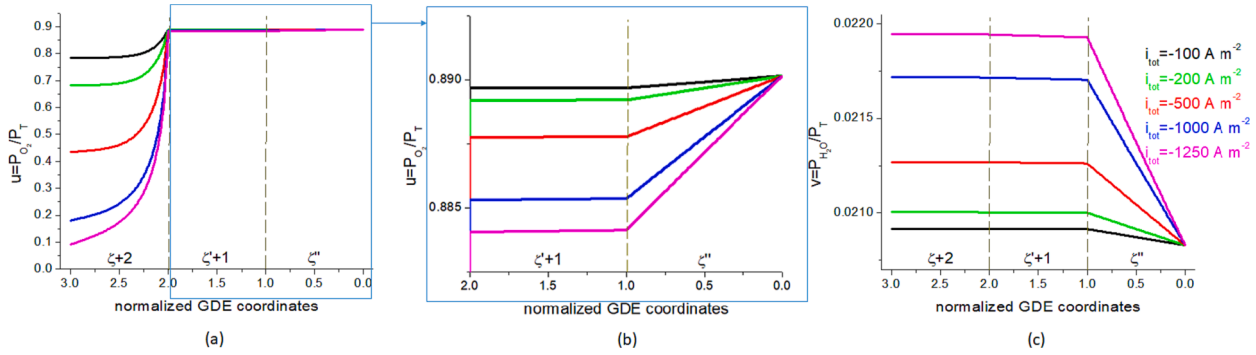

Fig. 5. Numerical solution of the non-dimensional partial pressure distributions u for O_2 (a, zoom in b) and v for H_2O (c) in BL, GDL and RL, as a function of applied current density i_{tot}. The parameter values used for the computations are reported in Table S1.

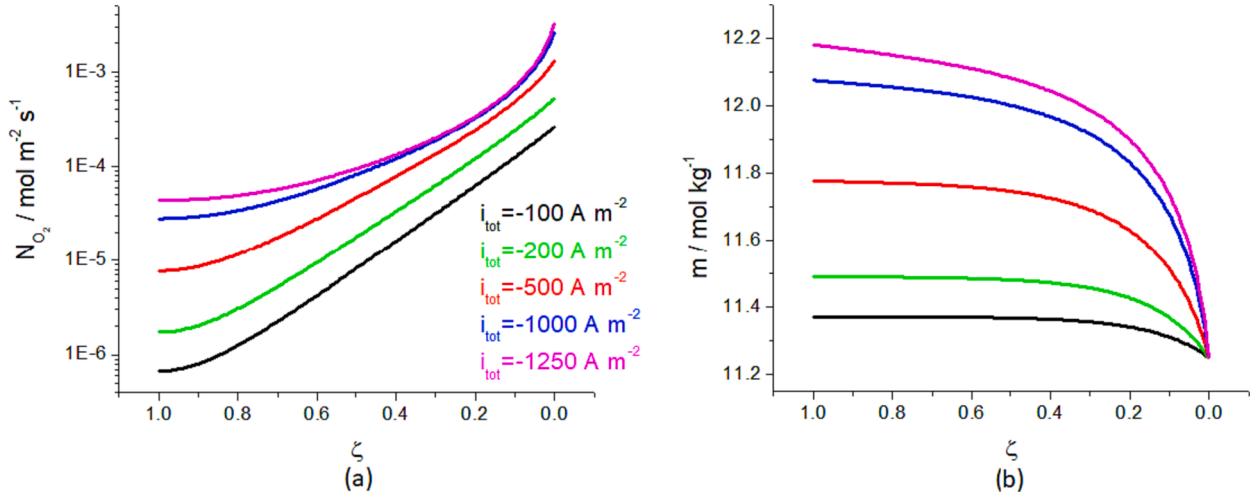

Fig. 6. Numerical solution of the oxygen flux N_{O_2} (a) and NaOH molality m (b) in the RL, as a function of applied current density i_{tot}. The other constant values used for the computations are reported in Table S1.

Maxwell-Stefan diffusion equations:

$$-\frac{1}{RT}\cdot\frac{dP_i}{dx}=\sum_{j\neq i}\frac{P_j\cdot N_i-P_i\cdot N_j}{P_T\cdot D_{i,j}^{g}} \tag{24}$$

where: P_i [N m^{-2}] is the partial pressure of the i-th gas on the mixture, x [m] is the space coordinate for a general 1D domain, N_i [mol m^{-2} s^{-1}] is the flux of the i-th gas, P_T [N m^{-2}] is the total pressure of the gas mixture and $D_{i,j}^{g}$ [m^2/s] is the Maxwell-Stefan free diffusion

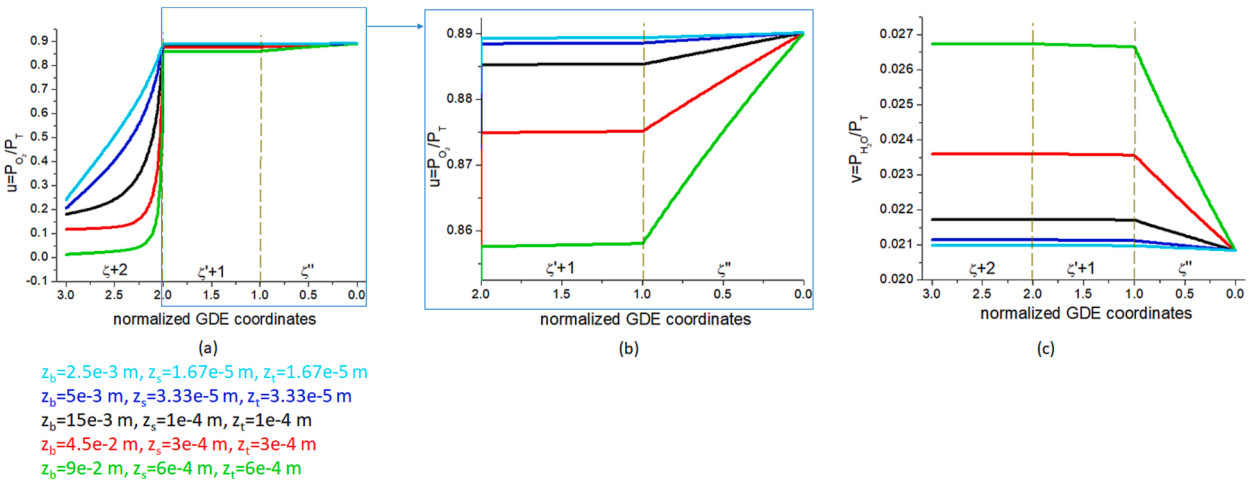

Fig. 7. Numerical solution of the non-dimensional partial pressure distributions u for O_2 (a, zoom in b) and v for H_2O (c) in BL, GDL and RL, obtained by varying the BL (z_b), GDL (z_s) and RL (z_t) thicknesses as indicated in the figure. The black plots correspond to the results reported in Fig. 5. All other parameter values are as reported in Table S1 and i_{tot} has been fixed to -1000 A m^{-2}.

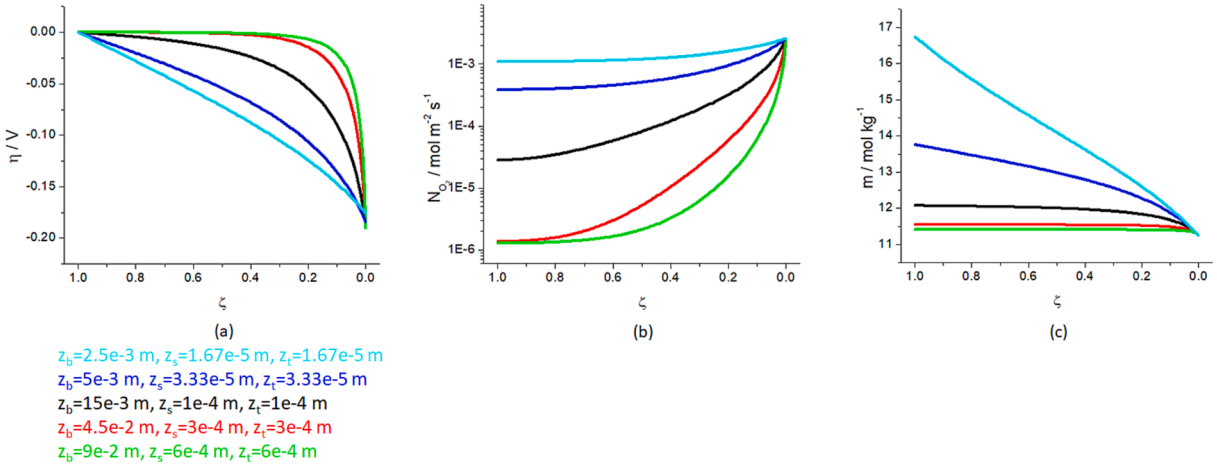

Fig. 8. Numerical solution of the overvoltage η (a), oxygen flux N_{O_2} (b) and NaOH molality m (c) in the RL, obtained by varying the BL (z_b), GDL (z_s) and RL (z_t) thicknesses as indicated in the figure. The black plots correspond to the results reported in Fig. 6. All other parameter values are as reported in Table S1 and i_{tot} has been fixed to -1000 A m^{-2}.

coefficient for the gas.

At variance with the gas chamber, the GDL and the active layer (AL) are porous media, whereby gas transport must be described in terms of Knudsen diffusion, combined with effective Maxwell-Stefan diffusion, described by:

$$-\frac{1}{RT}\cdot\frac{dP_i}{dx}=\frac{N_i}{D_i^{eff}}+\sum_{j\neq i}\frac{P_j\cdot N_i-P_i\cdot N_j}{P_T\cdot D_{i,j}^{eff}} \tag{25}$$

where D_i^{eff} and $D_{i,j}^{eff}$ [m^2/s] are the Knudsen and diffusion effective Maxwell-Stefan diffusion coefficients of species i, respectively.

The flux of oxygen is determined by the ORR reaction, thus:

$$N_{O_2}^g(z)\equiv N_{O_2}^g(z')\equiv N_{O_2}^g(z=0)=-\frac{i_{tot}}{4F} \tag{26}$$

This means that the flux of oxygen is everywhere constant in the BL and in the GDE, it is numerically equal to the flux at the entrance section of the BL and to the net ORR rate. Since the ORR is a cathodic process, $i_{tot}<0$ and the flux is oriented along the positive directions of coordinates z, z' and z''. It is worth noting that – as implied in [55] –, modelling gas-transport with Knudsen diffusion can lead to inconsistent solutions under the constant pressure hypothesis (Assumption (i)). In the present case, this inconsistency can be explicitly proved plugging the analytical solutions presented below in the above gas-transport equations. Specifically, by straightforward calculus, it can be shown that adopting jointy Assumptions (i)-(iii) of [1,2], Eq. (25) would hold only if $N_{O_2}^g(z)\equiv 0$. Since, as stated in the Introduction, it is beyond the scope of the present work to modify the implementation of TFAM as reported in [1,2], and mass transport in the gas phase is ancillary to the electrochemical problem at stake, having notified this formal criticality of TFAM as implemented in [1,2], we postpone the formulation of a novel consistent version of the mass-transport problem to a subsequent study.

2.3.2.1. Gas transport in Boundary Layer (BL): exact solution. Specializing, the Maxwell-Stefan mass-transport equations (Eq. (24)) for O_2 and H_2O, in the BL domain, applying Assumptions (i)-(iii), non-dimensionalizing them with the following definitions:

$$\zeta''=\frac{z''}{z_b} \tag{27}$$

$$u_{BL}=\frac{P_{O_2}(z'')}{P_T} \tag{28}$$

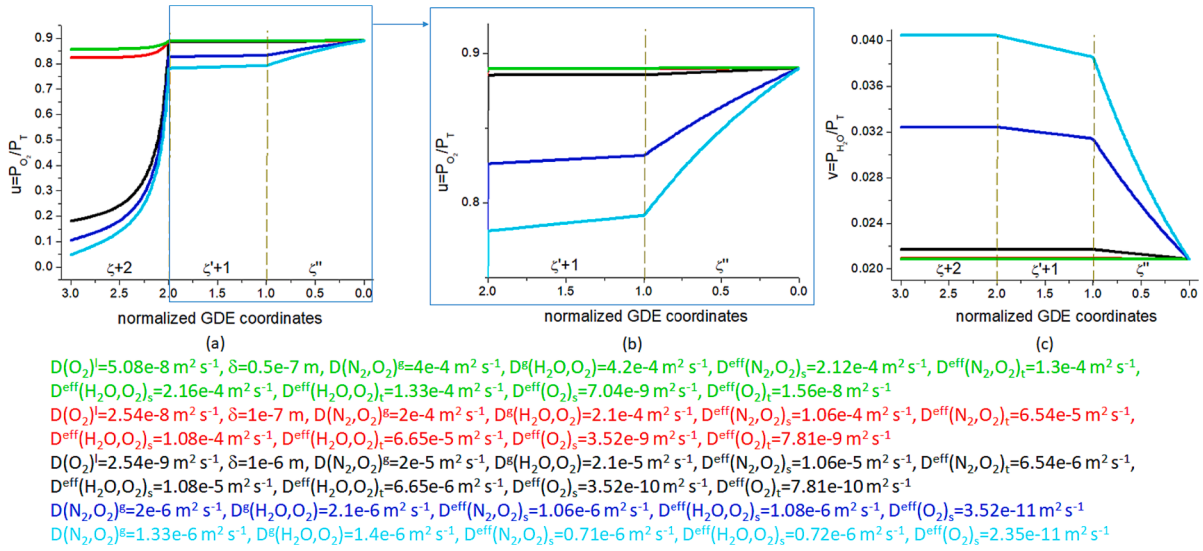

Fig. 9. Numerical solution of the non-dimensional partial pressure distributions u for O_2 (a, zoom in b) and v for H_2O (c) in BL, GDL and RL, obtained by varying the mass transport parameters as indicated in the figure with corresponding colours. The black plots correspond to the results reported in Fig. 5. All other parameter values are as reported in Table S1 and i_{tot} has been fixed to -1000 A m^{-2}.

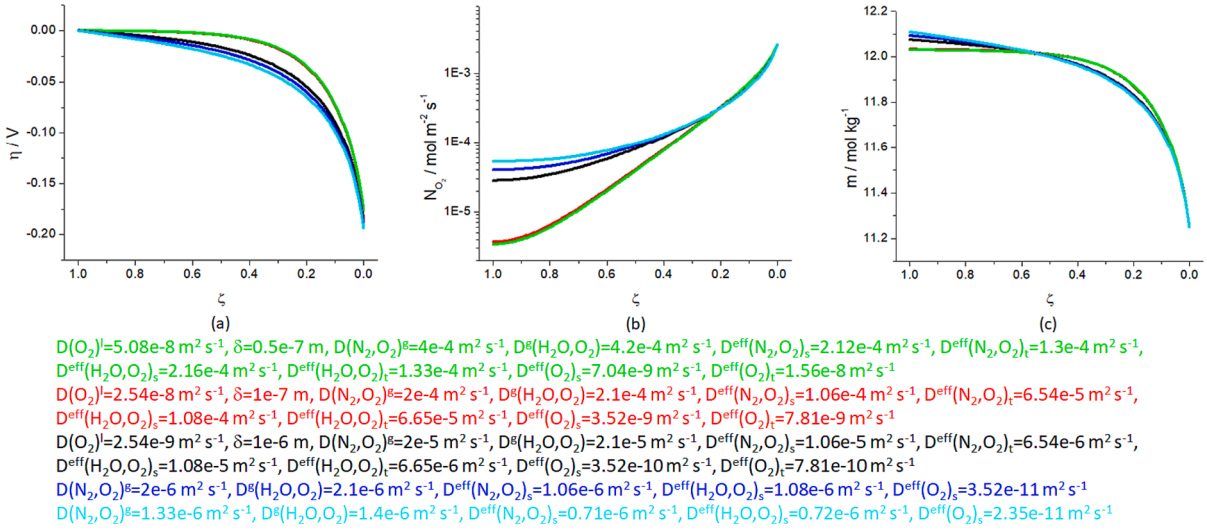

Fig. 10. Numerical solutions of the overvoltage η (a), oxygen flux N_{O_2} (b) and NaOH molality m (c) in the RL, obtained by varying the mass transport parameters as indicated in the figure. The black plots correspond to the result reported in Fig. 6. All other parameter values are as reported in Table S1 and i_{tot} has been fixed to -1000 A m^{-2}.

$$v_{BL} = \frac{P_{H_2O}(z'')}{P_T} \tag{29}$$

and setting the auxiliary constants:

$$\alpha_{BL} = \frac{N^g_{O_2} \cdot RT \cdot z_b}{P_T \cdot D^g_{O_2,N_2}} \tag{30}$$

$$\beta_{BL} = \frac{N^g_{O_2} \cdot RT \cdot z_b}{P_T} \cdot \left(\frac{1}{D^g_{O_2,N_2}} - \frac{1}{D^g_{O_2,H_2O}} \right) \tag{31}$$

$$\gamma_{BL} = \frac{N^g_{O_2} \cdot RT \cdot z_b}{P_T \cdot D^g_{O_2,H_2O}} \tag{32}$$

we obtain:

$$\frac{du_{BL}}{d\zeta''} = \alpha_{BL} \cdot (u_{BL} - 1) + \beta_{BL} \cdot v_{BL} \tag{33}$$

$$\frac{dv_{BL}}{d\zeta''} = \gamma_{BL} \cdot v_{BL} \tag{34}$$

The full derivation of Eqs. (33) and (34) is reported in Section S4 of the Supplementary Material.

Eq. (34) can be solved by separation of variables ([56] p. 31) with non-dimensional IC:

$$v_{BL}(\zeta'' = 0) = \frac{P_{H_2O,ext}}{P_T} \tag{35}$$

where $P_{H_2O,ext}$ is the partial pressure of H_2O vapour in the ambient external to the GDE, yielding:

$$v_{BL}(\zeta'') = v_{BL}(0) \cdot exp(\gamma_{BL} \cdot \zeta'') \tag{36}$$

This solution can be inserted into Eq. (33), giving a Bernoulli equation ([56] p. 49), that can be solved with IC:

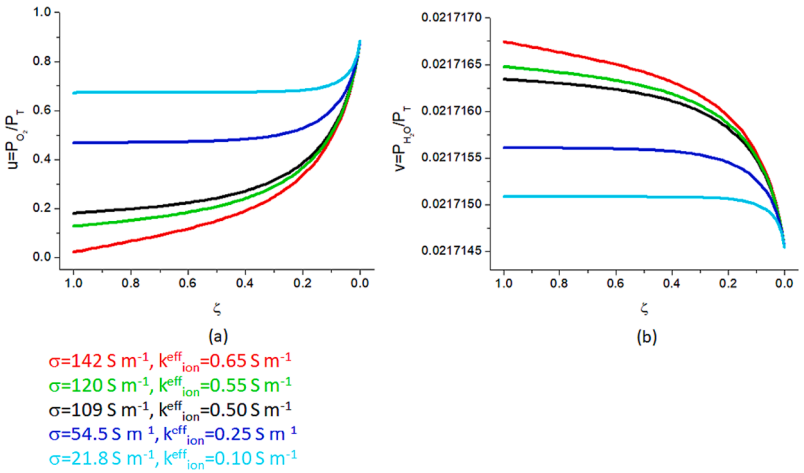

Fig. 11. Numerical solution of the non-dimensional partial pressure distributions u for O_2 (a) and v for H_2O (b) in RL, obtained by varying the electrical transport parameters as indicated in the figure by corresponding colours. The black plots correspond to the result reported in Fig. 5. All other parameter values are as reported in Table S1 and i_{tot} has been fixed to -1000 A m^{-2}.

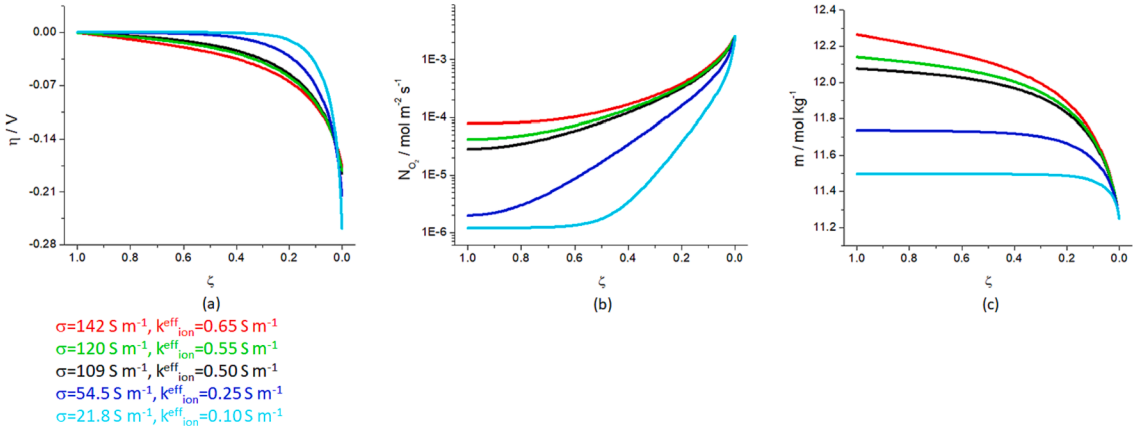

Fig. 12. Numerical solutions of the overvoltage η (a), oxygen flux N_{O_2} (b) and NaOH molality m (c) in the RL, obtained by varying the electrical transport parameters as indicated in the figure (see also Fig. 11). The black plots correspond to the result reported in Fig. 6. All other parameter values are as reported in Table S1 and i_{tot} has been fixed to -1000 A m^{-2}.

$$u_{BL}(\zeta'' = 0) = \frac{P_{O_2,ext}}{P_T} \tag{37}$$

where $P_{O_2,ext}$ is the partial pressure of O_2 in the ambient external to the GDE, yielding:

$$u_{BL}(\zeta'') = [u_{BL}(0) + v_{BL}(0) - 1]\cdot exp(\alpha_{BL}\cdot\zeta'') - v_{BL}(0)\cdot exp(\gamma_{BL}\cdot\zeta'') + 1 \tag{38}$$

Since $v_{BL}(0) < 1$, u_{BL} is a decreasing function of ζ'', coherently with the fact that O_2 is consumed in the RL. In keeping with this behaviour, since α_{BL} is positive, the partial pressure of H_2O increases from its value at the surface, as a result of the decrease of the partial pressure of O_2 resulting from the reaction occurring in the RL, under the constant pressure hypothesis (Assumption (i)).

2.3.2.2. Gas transport in the Gas-Diffusion Layer (GDL): exact solution. Specializing, the Maxwell-Stefan-Knudsen mass-transport equations (Eq. (25)) for O_2 and H_2O, in the GDL domain, applying Approximations (i)-(iii), non-dimensionalizing them with the following definitions:

$$\zeta'' = \frac{z'}{z_s} \tag{39}$$

$$u_{GDL} = \frac{P_{O_2}(z')}{P_T} \tag{40}$$

$$v_{GDL} = \frac{P_{H_2O}(z')}{P_T} \tag{41}$$

and setting the auxiliary constants:

$$\alpha_{GDL} = \frac{N^g_{O_2}\cdot RT\cdot z_s}{P_T\cdot D^{eff}_{O_2,N_2}} \tag{42}$$

$$\beta_{GDL} = \frac{N^g_{O_2}\cdot RT\cdot z_s}{P_T}\cdot\left(\frac{1}{D^{eff}_{O_2,N_2}} - \frac{1}{D^{eff}_{O_2,H_2O}}\right) \tag{43}$$

$$\gamma_{GDL} = \frac{N^g_{O_2}\cdot RT\cdot z_s}{P_T\cdot D^{eff}_{O_2,H_2O}} \tag{44}$$

$$\varepsilon_{GDL} = \frac{N^g_{O_2}\cdot RT\cdot z_s}{P_T}\cdot\left(\frac{1}{D^{eff}_{O_2}} + \frac{1}{D^{eff}_{O_2,N_2}}\right) \tag{45}$$

we obtain:

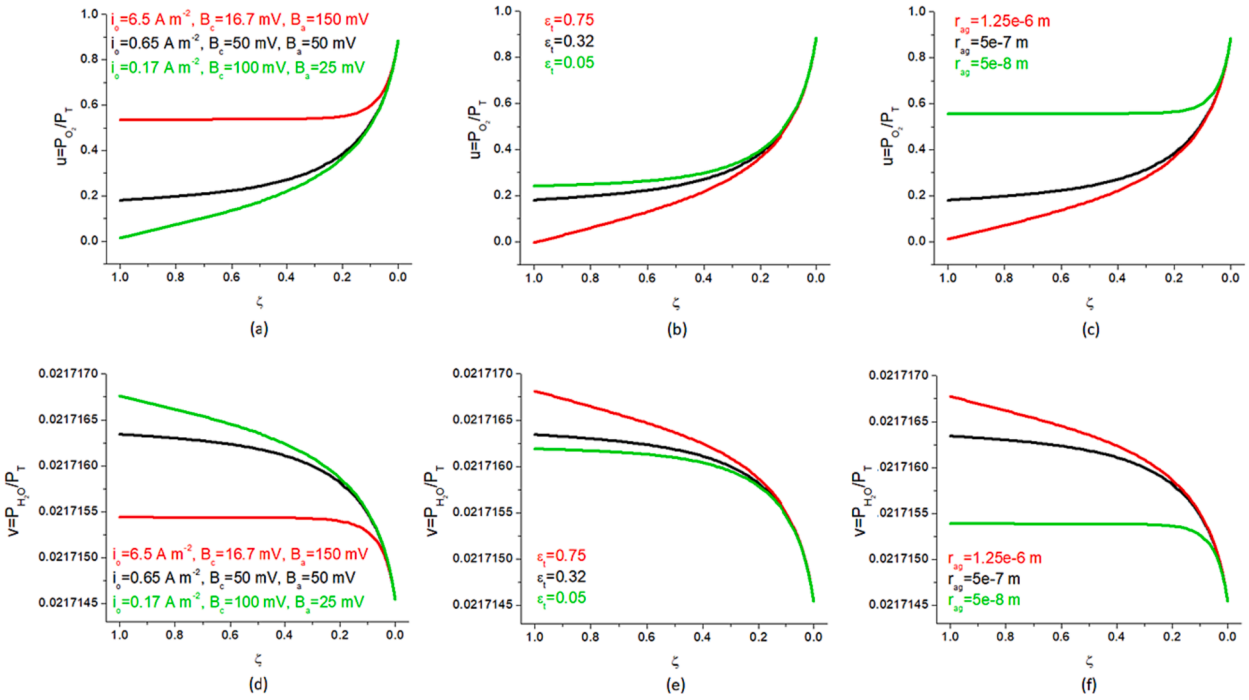

Fig. 13. Numerical solution of the non-dimensional partial pressure distributions u for O_2 (a-c) and v for H_2O (d-f) in RL, obtained by varying the electrokinetic parameters (a, d), the RL porosity (b, e) and the agglomerate radius dimensions (c, f) as indicated in the figure. The black plots correspond to the result reported in Fig. 5. All other parameter values are as reported in Table S1 and i_{tot} has been fixed to -1000 A m^{-2}.

$$\frac{du_{GDL}}{d\zeta'} = \alpha_{GDL}\cdot u_{GDL} + \beta_{GDL}\cdot v_{GDL} - \varepsilon_{GDL} \tag{46}$$

$$\frac{dv_{GDL}}{d\zeta'} = \gamma_{GDL}\cdot v_{GDL} \tag{47}$$

The full derivation of Eqs. (46) and (47) is reported in Section S5 of the Supplementary Material.

Again, Eq. (47) can be solved by separation of variables ([56] p. 31) with non-dimensional IC:

$$v_{GDL}(\zeta' = 0) = v_{BL}(\zeta'' = 1) \tag{48}$$

yielding:

$$v_{GDL}(\zeta') = v_{GDL}(0)\cdot exp(\gamma_{GDL}\cdot\zeta') \tag{49}$$

And again, with the same approach adopted for the solution in the BL domain, this solution can be inserted into Eq. (46), giving a Bernoulli equation ([56] p. 49), that can be solved with IC:

$$u_{GDL}(\zeta' = 0) = u_{BL}(\zeta'' = 1) \tag{50}$$

yielding:

$$u_{GDL}(\zeta') = \left[u_{GDL}(0) + v_{GDL}(0) - \frac{D^{eff}_{O_2,N_2}}{D^{eff}_{O_2} + D^{eff}_{O_2,N_2}}\right]\cdot exp(\alpha_{GDL}\cdot\zeta') - v_{GDL}(0)\cdot exp(\gamma_{GDL}\cdot\zeta') + \frac{D^{eff}_{O_2,N_2}}{D^{eff}_{O_2} + D^{eff}_{O_2,N_2}} \tag{51}$$

Of course, the right-hand sides of Eqs. (48) and (50) are derived from Eqs. (36) and (38).

For the same reasons discussed for u_{BL} and v_{BL}, coherently with the physics of the system, u_{GDL} and v_{GDL} are a decreasing and a growing function of ζ', respectively.

2.3.2.3. Gas transport and mass balances in the Reaction Layer (RL). As commented above, gas transport occurs in the gas region of the RL and a mass balance for O_2 in the AL has to be set up, to account for the ORR. In keeping with [1] and according to hypothesis (iii), the coupling of the gas region and of the AL within the RL is modelled assuming exchange equilibrium of H_2O between the electrolyte in the AL and the gas region. Following the same approach of previous Section, regarding the GDL domain, the complete Maxwell-Stefan-Knudsen mass-transport equations for O_2 and H_2O are formally identical to Eqs. (46) and (47), simply exchanging ζ for ζ', with the important difference that the oxygen flux here is a function of space $N^g_{O_2}(\zeta)$, as a result of the O_2 reaction in the AL. Thus, the gas-transport equations have to be coupled with an equation for the evolution of the oxygen flux, that can be written as:

$$\frac{dN^g_{O_2}}{d\zeta} = \frac{z_t}{nF}\cdot\frac{dS}{dV}\cdot i_R \tag{52}$$

with i_R defined in Eq. (20), and depending on the concentration of electroactive reagent, i.e. O_2 dissolved in the electrolyte phase, that is a function of the local partial pressure of O_2 in the gas region of the RL. With $n = 4$ accounting for the number of the exchanged electrons and the usual negative convention for the cathodic current, the slope of the O_2 flux is negative, in accord with the physics of the problem. Assuming exchange equilibrium for O_2 between the gas region (Assumption (iv)) and the AL in the gas region of the RL, this functional dependence can be expressed with Henry's law (see, e.g., [1]):

$$c(\zeta) = \frac{P_{O_2}(\zeta)}{H} \tag{53}$$

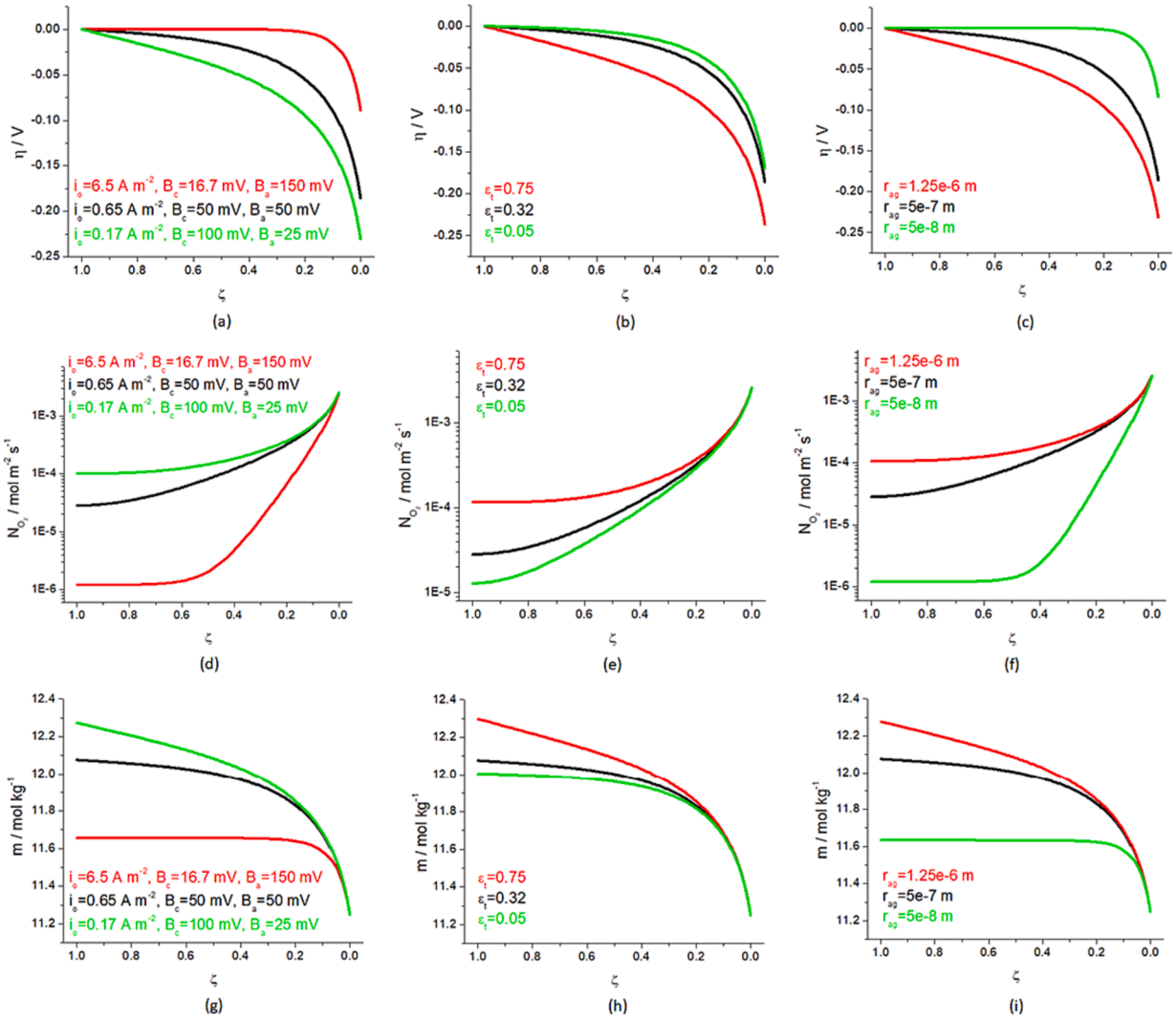

Fig. 14. Numerical solutions of the overvoltage η (a-c), oxygen flux N_{O_2} (d-f) and NaOH molality m (g-i) in the RL, obtained by varying the electrokinetic parmeters (a, d, e), the RL porosity (b, e, h) and the agglomerate radius dimensions (c, f, i) as indicated in the figure.. The black plots correspond to the result reported in Fig. 6. All other parameter values are as reported in Table S1 and i_{tot} has been fixed to -1000 A m^{-2}.

where H is the reciprocal of Henry's constant.

Setting:

$$u_{RL} = \frac{P_{O_2}(z)}{P_T} \tag{54}$$

$$v_{RL} = \frac{P_{H_2O}(z)}{P_T} \tag{55}$$

and combining Eqs. (20), (52) and (53), one obtains:

$$\frac{dN^g_{O_2}}{d\zeta} = \frac{z_t \cdot P_T}{H} \cdot \frac{dS}{dV} \cdot u_{RL} \cdot \frac{\frac{i_o}{c_o} \cdot \left(e^{\eta/B_a} - e^{-\eta/B_c}\right) \cdot \frac{D^l_{O_2}}{\delta}}{\frac{i_o}{c_o} \cdot \left(e^{\eta/B_a} - e^{-\eta/B_c}\right) + nF \cdot \frac{D^l_{O_2}}{\delta}} \tag{56}$$

η is the solution of Eq. (16), that, in turn, is coupled to the gas transport equation for P_{O_2}, to define the variable c of Eq. (20).

The coupled gas transport and mass balance equations for the non-dimensional partial pressures in the RL are thus:

$$\frac{du_{RL}}{d\zeta} = N^g_{O_2}(\zeta) \cdot [\alpha_{RL} \cdot u_{RL} + \beta_{RL} \cdot v_{RL} - \varepsilon_{RL}] \tag{57}$$

$$\frac{dv_{RL}}{d\zeta} = \gamma_{RL} \cdot N^g_{O_2}(\zeta) \cdot v_{RL} \tag{58}$$

where:

$$\alpha_{RL} = \frac{RT \cdot z_t}{P_T \cdot D^{eff}_{O_2,N_2}} \tag{59}$$

$$\beta_{RL} = \frac{RT \cdot z_t}{P_T} \cdot \left(\frac{1}{D^{eff}_{O_2,N_2}} - \frac{1}{D^{eff}_{O_2,H_2O}}\right) \tag{60}$$

$$\gamma_{RL} = \frac{RT \cdot z_t}{P_T \cdot D^{eff}_{O_2,H_2O}} \tag{61}$$

$$\varepsilon_{RL} = \frac{RT \cdot z_t}{P_T} \cdot \left(\frac{1}{D^{eff}_{O_2}} + \frac{1}{D^{eff}_{O_2,N_2}}\right) \tag{62}$$

Eqs. (57) and (58) can be solved with the ICs:

$$u_{RL}(\zeta = 0) = u_{GDL}(\zeta' = 1) \tag{63}$$

$$v_{RL}(\zeta = 0) = v_{GDL}(\zeta' = 1) \tag{64}$$

$$N^g_{O_2}(\zeta = 0) = N^g_{O_2}(\zeta' = 1) \tag{65}$$

ICs that express continuity are the only condition required for the solution of the pressure equations (Eqs. (63) and (64)). Regarding the

flux equation for O_2, apart from merely mathematical reasons, it is clear that the continuity condition Eq. (65) is sufficient to fully determine $N^g_{O_2}(\zeta)$, because, physically, no restrictions are placed on this variable at $\zeta = 1$ since O_2 is exchanged with the liquid phase in the whole RL domain.

The full coupled gas-transport (Eqs. (57) and (58)), mass balance (Eq. (56)) and overvoltage distribution (Eqs. (16) and (20)) problem for the RL can be solved numerically with the ICs (Eqs. (63), (64), (65), (21) and (22)), the first two of which obtained from the analytical solutions of the gas-transport equations for the BL (Eqs. (36) and (38)) and the GDL (Eqs. (49) and (51)). Details will be provided below. Moreover, simplified, semi-analytical self-consistent solutions can be obtained, that enable a transparent physical analysis and parametric study: this is the object of Section S6 of the Supplementary Material.

2.3.3. Mass transport in the liquid phase of the AL

Equations for mass transport in the liquid phase of the AL can be derived from the solution of the gas transport in the gas region of the AL, by straightforward post-processing, based on the solution of the O_2 flux $N^g_{O_2}$. Since O_2 is consumed only in the AL and phase-exchange equilibrium for O_2 is assumed (Assumption (iv)), $N^g_{O_2}$ is numerically equivalent to the O_2 flux in the liquid phase of the AL.

2.3.3.1. Transport of H_2O in the liquid phase of the AL. From the material balance corresponding to the four-electron O_2 reduction mechanism (Assumption (vi)):

$$O_2 + 2H_2O + 4e^- \rightarrow 4OH^- \tag{66}$$

whence it results:

$$N^l_{H_2O}(\zeta) = N^l_{H_2O}(1) + 2 \cdot N^g_{O_2}(\zeta) \tag{67}$$

where $N^l_{H_2O}(1) = 0$, since the flux of water at the current feeder/GDE interface must be zero.

The approximated analytical solution Eq. (S39) can be employed to obtain an analytical solution for the H_2O flux:

$$N^l_{H_2O}(\zeta) = -\frac{i_{tot}}{2F} \cdot exp\left(-\frac{\zeta}{\tilde{\tau}}\right) \tag{68}$$

A positive flux of H_2O (that is $-i_{tot} > 0$) is, of course, coherent with the consumption of water accompanying O_2 reduction.

2.3.3.2. Transport of OH^- in the liquid phase of the AL. Again, from Eq. (66), one obtains:

$$N^l_{OH^-}(\zeta) = N^l_{OH^-}(1) - 4 \cdot N^g_{O_2}(\zeta) \tag{69}$$

where $N^l_{OH^-}(1) = 0$, since the flux of OH^- at the current feeder/GDE interface must be zero.

Again, the approximated analytical solution Eq. (S39) can be employed to obtain an analytical solution for the OH^- flux:

$$N^l_{OH^-}(\zeta) = \frac{i_{tot}}{F} \cdot exp\left(-\frac{\zeta}{\tilde{\tau}}\right) \tag{70}$$

A negative flux of OH^- is ($-i_{tot} > 0$), of course, coherent with the production of OH^- accompanying O_2 reduction.

2.3.3.3. Transport of NaOH in the liquid phase of the AL. Following the treatment of [1], the NaOH molality profile, being $[NaOH](\zeta) = m(\zeta) \cdot \rho$ - with m [mol kg^{-1}] the molality of NaOH and ρ [kg m^{-3}] the density of the solution - can be modelled in terms of the Maxwell-Stefan equation (see Eqs. (S21) and (S22) and the concentrated solution theory (e.g. [40]):

$$\frac{dm}{d\zeta} = \frac{\frac{m}{2RT} \cdot \frac{d\mu_N}{d\zeta}}{1 + m \cdot ln10 \cdot \frac{dLog\gamma}{dm}} \tag{71}$$

with μ_N [J K^{-1} mol^{-1}] the chemical potential of NaOH and γ [1] the activity coefficient of NaOH.

From the Maxwell-Stefan equation:

$$\frac{d\mu_N}{d\zeta} = \frac{RT}{\frac{\rho}{M_A} \cdot (1 - m \cdot M_N + 2 \cdot m \cdot M_A)} \cdot \left(\frac{N^l_{H_2O}}{D_{A,+}} + \frac{N^l_{H_2O} - \frac{1 - m \cdot M_N}{m \cdot M_A} \cdot N^l_{OH}}{D_{A,-}} \cdot \right) \tag{72}$$

where $N^l_{H_2O}$ and N^l_{OH} are the solutions of Eqs. (67) and (69), respectively. $\frac{dLog\gamma}{dm}$ is tabulated in [57].

The full derivation of Eq. (71) and Eq. (72), as well as of an expression for $dLog(\gamma)/dm$ (Eq. S58), are provided in Section S7 of the Supplementary Material.

According to Assumption (v), Eq. (71) can be solved numerically with the IC:

$$m(\zeta = 0) = m_{bulk}. \tag{73}$$

In our numerical computation we have used $m_{bulk} = 11.25$ mol kg^{-1}.

3. Numerical approximation of the full problem

The full problem is solved numerically with a MATLAB script, employing standard ODE solvers for initial and boundary value problems (like Runge-Kutta and collocation schemes, respectively) and the self-consistent iterative scheme expounded in Fig. 4. Convergence is typically achieved with four iterations. In Figs. 5 and 6, we report a set of representative profiles - in the three regions of the GDE - of gas partial pressures, O_2 flux and molality, as a function of the applied current density, employing the parameter values reported in Table S1 of the Supplementary Material, corresponding to literature results and original estimates or measurements, as specified in the caption. The expected trends are retrieved, with quantitative values in the expected physical range. In fact, increasing current densities yield progressively lower O_2 partial pressures (Fig. 5a and 5b) and higher water concentrations (Fig. 5c) in all the GDE domains.

In correspondence, in the RL, the O_2 flux (Fig. 6a) and the OH^- concentration (Fig. 6b) increase. More results, spanning a reasonable region of the parameter space with a heuristic selection are reported in Figs. 7-14. Figs. 7 and 8 report the effect of varying jointly the thicknesses of the BL (z_b), GDL (z_s) and RL (z_t). From Fig. 7 it can be noticed that increasing the thicknesses leads, as expected, to the combined decrease of $p(O_2)$ and increase of $p(H_2O)$ over all the regions and to a more pronounced O_2 consumption and H_2O production in the RL. In correspondence, the overvoltage (η) drop is progressively more localized close to the RL/GDL interface (Fig. 8a), the O_2 flux increases (Fig. 8b) and the concentration of OH^- increases inside the RL (Fig. 8c). Figs. 9 and 10 report the impact of the mass-transport conditions. With respect to the reference case of Figs. 5 and 6, in this case, the diffusion coefficients in all domains are increased and the boundary layer thickness in the RL is decreased, while, only the diffusion coefficients on the BL and GDL are decreased, because the reference current density is close to the limiting current density. As expected, $p(O_2)$ (Fig. 9a and 9b) decreases and $p(H_2O)$ (Fig. 9c) increases with parameter values expressing favoured diffusion. Consistently, lower η values (Fig. 10a) and higher O_2 fluxes (Fig. 10b) are computed. In this particular instance, the OH^- concentration (Fig. 10c) exhibits a qualitative change in depth dependence between the case in which all mass-transport parameters are increased (green and red plots) and that in which only mass-transport in the BL and GDL are decreased (blue and light blue plots). In the former case, increasing mass transport also in the RL results in a smoother distribution of the reaction product, while in the latter a steeper gradient develops corresponding to readier transport of reagent to the RL. In Figs. 11 and 12 we investigate the consequence of varying the electrical transport parameters (electronic and ionic conductivities) around the value employed for the computations of Figs. 5 and 6. In Fig. 11 we show

only results corresponding to the RL, because the $p(O_2)$ and $p(H_2O)$ profiles in the BL and GDL domains are not affected by varying the conductivities. Increasing electrical transport clearly favours reactivity, bringing about systematic decreases in $p(O_2)$ (Fig. 11a) and increases in $p(H_2O)$ (Fig. 11b). Coherently, favoured electrical transport brings about lower and more distributed electrochemical polarizations η (Fig. 12a), higher O_2 fluxes (Fig. 12b) and OH^- concentrations (Fig. 12c), with higher gradients. The effects of electrokinetic parameters (i_o, B_c and B_a), porosity ε_t and electrocatalyst grain dimensions r_{ag} are evaluated in Figs. 13 and 14. Fig. 13 reports the impact of these parameters on $p(O_2)$ and $p(H_2O)$. Increasing the cathodic electrokinetics (Fig. 13a, c: higher i_o, lower B_c and higher B_a) favours a more homogeneous distribution of reagent and reaction product. Increasing the porosity (Fig. 13b, d) and decreasing the electrocatalyst grain size (Fig. 13c, f) lead to higher RL activity, witnessed by lower $p(O_2)$ and higher $p(H_2O)$ values. Increasing electrokinetics (Fig. 14a) yields lower overvoltages, but higher porosities, while lower particle dimensions, correlated through Eq. (3), give rise to higher η values (Fig. 14b, c), owing to a subtle combination of electrochemical rate and effective conductance effects. Enhanced electrokinetics leads to a confinement of the O_2 flux close to the RL/GDL interface (Fig. 14d) and to a lower OH^- concentration gradient (Fig. 14g). Increasing the porosity (Fig. 14e) and reducing the electrocatalytic particle dimensions (Fig. 14f) results in a higher O_2 flux. The OH^- concentration is higher the larger the porosity (Fig. 14h) and the smaller the electrocatalyst particle dimensions (Fig. 14i), coherenrly with a larger activity of the RL.

The above set of results shows that the full solution can be obtained varying the parameter values within physically reasonable ranges, obtaining the correct trends in terms of space and current dependence. Systematic use of this approach for systematic sensitivity analysis and parametric identification, carried out with deep learning approaches [58], will be made in subsequent work for the rationalization of experimental data that we are systematically generating with a novel approach for the fabrication of highly efficient and durable GDEs for alkaline metal-air batteries [59].

4. Conclusions

This paper restates, in full and explicit form, the Thin-Film Flooded Agglomerate Model (TFAM) for Air Cathodes implementing the Oxygen Reduction Reaction (ORR), in the stationary, isothermal version, originally proposed in [1,2]. The specific scope of this work is to make the TFAM concretely usable for the GDE science and technology community, in view of systematically linking electrode architecture factors – with their experimental assessment by imaging and scattering methods – and electrochemical performance.

The complete physico-chemical derivation is reported with the corresponding formalism, presented perspicuously. The full numerical solution and a complete simplified analytical integration are presented and discussed in self-contained form, giving all the mathematical details, required to replicate the computations.

Special care is given to communicate in an uncompromising way contents that seem trivial, but concretely are stumbling block is the implementation of the model, including the precise numerical values of all model parameters and their origin, with consistent dimensions.

Finally, a selection of representative solutions is presented and discussed.

A comprehensive sensitivity analysis, eased by the extensive analytical elaboration we offer in the present work, and efficient approaches to systematic parameter identification for original experimental data, will be the object of a follow up paper.

CRediT authorship contribution statement

Benedetto Bozzini: Conceptualization, Methodology, Software, Validation, Formal analysis, Investigation, Data curation, Writing – original draft, Writing – review & editing. **Ivonne Sgura:** Methodology, Software, Formal analysis.

Declaration of Competing Interest

The authors declare that they have no known competing financial interests or personal relationships that could have appeared to influence the work reported in this paper.

Acknowledgments

i) The Authors gratefully acknowledge Alessandro Alleva's (Department of Energy, Politecnico di Milano) contribution to the evaluation of the numerical values of the model constants.

ii) This study was carried out within the MOST – Sustainable Mobility Center and received funding from the European Union Next-GenerationEU (PIANO NAZIONALE DI RIPRESA E RESILIENZA (PNRR) – MISSIONE 4 COMPONENTE 2, INVESTIMENTO 1.4 – D.D. 1033 17/06/2022, CN00000023). This manuscript reflects only the authors' views and opinions, neither the European Union nor the European Commission can be considered responsible for them.

Appendix A. Supplementary data

Supplementary data to this article can be found online at https://doi.org/10.1016/j.jelechem.2023.117855.

References

[1] S. Pinnow, N. Chavan, T. Turek, J. Appl. Electrochem. 41 (2011) 1053.
[2] D. Franzen, M.C. Paulisch, B. Ellendorff, I. Manke, T. Turek, Electrochim. Acta 375 (2021), 137976.
[3] L.C. Brée, K. Perrey, A. Bulan, A. Mitsos, AIChE J 65 (2019) e16352.
[4] S. Lakshmanan, T. Murugesan, Clean Technol. Environ, Policy, 16 (2014) 225.
[5] I. Moussallem, J. Jörissen, U. Kunz, S. Pinnow, T. Turek, J. Appl. Electrochem. 38 (2008) 1177.
[6] F. Kubannek, T. Turek, U. Krewer, Chem. Ing. Tech. 91 (2019) 720.
[7] M. Röhe, F. Kubannek, U. Krewer, ChemSusChem 12 (2019) 2373.
[8] R.C. Burshtein, V.S. Markin, A.G. Pshenichnikov, V.A. Chismadgev, Y.G. Chirkov, Electrochim. Acta 9 (1964) 773.
[9] F.G. Will, J. Electrochem. Soc. 110 (1963) 152.
[10] L.G. Austin, M. Ariet, R.D. Walker, G.B. Wood, R.H. Comyn, Ind. Eng. Chem. Fundamen. 4 (1965) 321.
[11] S. Srinivasan, H.D. Hurwitz, Electrochim Acta 12 (1967) 495.
[12] E.A. Grens II, C.W. Tobias, Electrochim. Acta 10 (1965) 761.
[13] E.A. Grens II, Electrochim. Acta 15 (1970) 1047.
[14] J. Giner, C. Hunter, J. Electrochem. Soc. 116 (1969) 1124.
[15] M.B. Cutlip, Electrochim. Acta 20 (1975) 767.
[16] R.P. Iczkowski, M.B. Cutlip, J. Electrochem. Soc. 127 (1980) 1433.
[17] P. Björnbom, Electrochim. Acta 32 (1987) 115.
[18] S.C. Yang, M.B. Cutlip, P. Stonehart, Electrochim. Acta 35 (1990) 869.
[19] S.C. Yang, P. Björnbom, Electrochim. Acta 37 (1992) 1831.
[20] X.L. Wang, S. Koda, Denki Kagaku 65 (1997) 1014.
[21] J. Newman, Adv. Electrochem. Electrochem. Eng. 5 (1967) 87.
[22] N. Chavan, S. Pinnow, G.D. Polcyn, T. Turek, J. Appl. Electrochem. 45 (2015) 899.
[23] M. Röhe, D. Franzen, F. Kubannek, B. Ellendorff, T. Turek, U. Krewer, Electrochim. Acta 389 (2021), 138693.
[24] P. Kunz, M. Hopp-Hirschler, U. Nieken, Chem. Ing. Tech. 91 (2019) 883.
[25] B. Horstmann, T. Danner, W.G. Bessler, Energ. Environ. Sci. 6 (2013) 1299.
[26] I. Moussallem, S. Pinnow, N. Wagner, T. Turek, Chem. Eng. Process. 52 (2012) 125.
[27] S. Kandaswamy, A. Sorrentino, S. Borate, L.A. Živković, M. Petkovska, T. Vidaković-Koch, Electrochim. Acta 320 (2019), 134517.
[28] M. Röhe, A. Botz, D. Franzen, F. Kubannek, B. Ellendorff, D. Öhl, W. Schuhmann, T. Turek, U. Krewer, ChemElectroChem 6 (2019) 5671.
[29] A. Löwe, C. Rieg, T. Hierlemann, N. Salas, D. Kopljar, N. Wagner, E. Klemm, ChemElectroChem 6 (2019) 4497.
[30] D. Franzen, C. Krause, T. Turek, ChemElectrroChem 8 (2021) 2186.
[31] A. Botz, J. Clausmeyer, D. Öhl, T. Tarnev, D. Franzen, T. Turek, W. Schuhmann, Angew. Chem. Int. Ed. 57 (2018) 12285.
[32] T. Danner, B. Horstmann, D. Wittmaier, N. Wagner, W.G. Bessler, J. Power Sources 264 (2014) 320.
[33] U. Sahapatsombut, H. Cheng, K. Scott, J. Energy Storage 7 (2016) 220.
[34] X.-Y. Liu, X.-Z. Xu, Appl. Math. Mech. - Engl. Ed. 34 (2013) 571.
[35] T. Danner, S. Eswara, V.P. Schulz, A. Latz, J. Power Sources 324 (2016) 646.
[36] B.G. Higgins and H. Binous, "Binary Diffusion Coefficients for Gases", http://demonstrations.wolfram.com/BinaryDiffusionCoefficientsForGases, published: February 21th, 2013.

[37] S. Brimaud, E. Marini, M. Liebert, F. Rossi, D. Oliveira De Souza, P. Baumli, G. Aquilanti, F. Regnet, I. Lüdeking, B. Bozzini, L. Jörissen, J. Power Sources 546 (2022), 231879.
[38] J. Newman, W. Tiedemann, AIChE J 21 (1975) 25.
[39] R. Alkire, P.K. Ng, J. Electrochem. Soc. 124 (1977) 1220.
[40] Y. Volkman, Electrochim. Acta 24 (1979) 1145.
[41] W.G. Sunu, D.N. Bennion, J. Electrochem. Soc. 127 (1980) 2007.
[42] J. Van Zee, R.E. White, J. Electrochem. Soc. 130 (1983) 2003.
[43] K. Scott, J. Appl. Electrochem. 13 (1983) 709.
[44] E.C. Dimpault-Darcy, T.V. Nguyen, R.E. White, J. Electrochem. Soc. 135 (1998) 278.
[45] O. Lanzi, U. Landau, J. Electrochem. Soc. 137 (1990) 585.
[46] Z. Mao, P.D. De Vidts, R.E. White, J. Newman, J. Electrochem. Soc. 141 (1994) 54.
[47] M. Doyle, J. Newman, Electrochim. Acta 40 (1995) 2191.
[48] T. Doherty, J.G. Sunderland, E.P.L. Roberts, D.J. Pickett, Electrochim. Acta 41 (1996) 519.
[49] P. De Vidts, R.E. White, J. Electrochem. Soc. 144 (1997) 1343.
[50] F. Brosa Planella, W. Ai, A.M. Boyce, A. Ghosh, I. Korotkin, S. Sahu, V. Sulzer, R. Timms, T.G. Tranter, M. Zyskin, S.J. Cooper, J.S. Edge, J.M. Foster, M. Marinescu, B. Wu, G. Richardson, Prog. Energy 4 (2022), 042003.
[51] J.C. Bui, E.W. Lees, L.M. Pant, I.V. Zenyuk, A.T. Bell, A.Z. Weber, Chem. Rev. 122 (2022) 11022.
[52] A. Wolf, E. Baudrin, H. Nirschl, Energy Technol. 2300175 (2023).
[53] B. Bozzini, J. Chem. Edu. 77 (2000) 100.
[54] P. Costamagna, P. Costa, V. Antonucci, Electrochim. Acta 43 (1998) 375.
[55] A. Bertei, C. Nicolella, J. Power Sources 279 (2015) 133.
[56] M.L. Krasnov, A.I. Kiselyov, G.I. Makarenko, A Book of Problems in Ordinary Differential Equations, Mir publishers, Moskow, 1981.
[57] G. Åkerlöf, G. Kegeles, J. Am. Chem. Soc. 62 (1940) 620.
[58] I. Sgura, L. Mainetti, F. Negro, M.G. Quarta, B. Bozzini, Journal of Comput. Sci. 66 (2023), 101900.
[59] Y. Salman, S. Waseem, A. Alleva, P. Banerjee, V. Bonanni, E. Emanuele, R. Ciancio, A. Gianoncelli, G. Kourousias, A. Li Bassi, A. Macrelli, E. Marini, B. Bozzini, Electrochim. Acta 469 (2023), 143246.